ADWR 854
8 June 2005 Disk Used
ARTICLE IN PRESS
No. of Pages 18, DTD = 5.0.1

Available online at www.sciencedirect.com
SCIENCE DIRECT®

Advances in Water Resources

Advances in Water Resources xxx (2005) xxx–xxx

www.elsevier.com/locate/advwatres

Multi-functional heat pulse probe measurements of coupled vadose zone flow and transport

Annette P. Mortensen [a], Jan W. Hopmans [b,*], Yasushi Mori [c], Jirka Šimůnek [d]

[a] Geological Institute, Copenhagen University, Øster Voldgade 10, 1350 Copenhagen, Denmark
[b] Hydrology Program, Department of Land, Air and Water Resources, University of California, 123 Veihmeyer Hall, Davis, CA 95616, USA
[c] Faculty of Life and Environmental Science, Shimane University, Matsue 690-8504, Japan
[d] Department of Environmental Sciences, University of California, Riverside, CA 92521, USA

Received 1 March 2005; accepted 14 March 2005

Abstract

Simultaneous measurement of coupled water, heat, and solute transport in unsaturated porous media is made possible with the multi-functional heat pulse probe (MFHPP). The probe combines a heat pulse technique for estimating soil heat properties, water flux, and water content with a Wenner array measurement of bulk soil electrical conductivity (EC_{bulk}). To evaluate the MFHPP, we conducted controlled steady-state flow experiments in a sand column for a wide range of water saturations, flow velocities, and solute concentrations. Flow and transport processes were monitored continuously using the MFHPP. Experimental data were analyzed by inverse modeling of simultaneous water, heat, and solute transport using an adapted HYDRUS-2D model. Various optimization scenarios yielded simultaneous estimation of thermal, solute, and hydraulic parameters and variables, including thermal conductivity, volumetric water content, water flux, and thermal and solute dispersivities. We conclude that the MFHPP holds great promise as an excellent instrument for the continuous monitoring and characterization of the vadose zone.

Keywords: Heat pulse probe; Unsaturated flow; Heat transport; Solute transport; Vadose zone properties; Water content; Water flux; Dispersion

1. Introduction

Multi-functional measurements of vadose zone processes have received increased attention over the past few years. New sensors are being developed, by which several already well-known measurement techniques are combined into a single device. Examples of multi-functional instruments include a combined TDR and tensiometer probe [44], a combined TDR and heat pulse probe [28], and a combined heat pulse probe with a Wenner array [25], as used in the current study. Also multi-functional tracing techniques have been developed that apply several tracers with different properties simultaneously (e.g., [27]). The overall motivation for the development of these multi-functional techniques is to achieve an improved characterization of flow and transport processes. Several benefits are achieved by combining measurements. First, by measuring several parameters at the same time and place, the coupling of related transport properties are determined in concert, thereby allowing examination of the nature of their interdependency, such as for the coupled transport of water and solute, and water and heat. Second, by using the same instrument for various measurements within approximately the same measurement volume at about the same time, the need to interpolate different measurement types in space and time is largely eliminated.

* Corresponding author. Tel.: +1 530 752 3060; fax: +1 530 752 5262.
E-mail address: jwhopmans@ucdavis.edu (J.W. Hopmans).

0309-1708/$ - see front matter © 2005 Published by Elsevier Ltd.
doi:10.1016/j.advwatres.2005.03.017

Thirdly, simultaneous analysis of flow and transport using combined soil measurements of water content, temperature, and solute concentration, decreases parameter uncertainty [24,37,39]. Thus, using multi-functional measurement techniques allows determination of interdependent soil properties and processes, providing an improved understanding of coupled flow and transport.

The presented multi-functional heat pulse probe (MFHPP) originates from the dual-probe heat pulse (DPHP) method developed by Campbell et al. [11]. By inducing a short heat pulse from one sensor needle and measuring the temperature response at a second sensor, the soil thermal properties (i.e., heat capacity, C; thermal conductivity, λ_0; and thermal diffusivity, κ) and the water content, θ, were estimated. This method has been tested in both laboratory settings (e.g. [2,4–7]) and in field soils [16,40]. Over the past few years, the DPHP probe has been refined and was developed into various multi-sensor probes that are capable of simultaneous measuring a suite of soil properties. The so-called thermo-TDR was developed by combining the DPHP probe with TDR technology, to achieve a probe that in addition to soil thermal properties also estimates soil solute concentration from the simultaneous measurement of the bulk soil electrical conductivity (EC_{bulk}) [28,30,32,34]. The potential of measuring EC_{bulk} using a modified heat pulse probe was shown by Bristow et al. [8], by including two extra sensor needles in the DPHP probe to create a so-called four-electrode Wenner array. Since EC_{bulk} measurements are dependent on both solute concentrations and water contents, EC_{bulk} is an integral variable characterizing both water flow and solute transport that can be beneficially used to simultaneously estimate soil hydraulic and solute transport parameters [21,37].

By inclusion of an extra temperature sensor to measure both the temperature responses at the upstream and downstream end of the heater sensor, Ren et al. [33] demonstrated the added benefit of water flux estimation. The resulting three rod heat pulse probe was successfully used to measure water fluxes in the range of 1–3 m d^{-1}, but significantly underestimated larger fluxes [33]. In their modeling and sensitivity study, Hopmans et al. [19] suggested that this underestimation could be caused by the neglection of thermal dispersion at these larger flow velocities, and they showed that more accurate water flux estimates could be obtained, if an extra transverse thermistor needle was included in the HPP to take into account thermal dispersion. The multi-functional heat pulse probe (MFHPP) of the current study combines this type of heat sensor with a four-needle Wenner array. As demonstrated by Mori et al. [25,26], the MFHPP allow estimation of the soil thermal properties (i.e., heat conduction, thermal conductivity, and thermal diffusivity), simultaneously with the soil water properties (water content and water flux). Furthermore, the MFHPP estimates EC_{bulk} from Wenner array measurements, from which the soil's solute concentration and water content can be determined.

In this study, the MFHPP technique was applied in flow and transport column experiments for the simultaneous and coupled measurement of water, heat, and solute transport variables and properties. Controlled steady-state flow experiments through variably-saturated sand were conducted for a range of water flux, water saturation, and solute concentration values. Heat pulse and EC_{bulk} measurements were analyzed with inverse modeling using a modified version of the HYDRUS-2D code [19,36]. The main objective of the presented study was to evaluate the MFHPP as a means to fully characterize coupled soil water flow, heat, and solute transport properties and processes.

2. Theory

Soil thermal and hydraulic properties were evaluated from analysis of temperature responses of the thermistors of the MFHPP, solving for heat transport by both conduction and convection. Solution of solute transport is needed for interpretation of bulk soil electrical conductivity (EC_{bulk}) measurements. The presented analysis will solve the coupled heat, water, and solute transport equations using HYDRUS-2D [36]. Although we will assume that both water and solute transport is one-dimensional in our experiments, the two-dimensional form of the heat flow equation is required to account for heat transport in the vertical and lateral directions between the sensors of the MFHPP [19].

2.1. Heat transport

Under the assumption of instantaneous heat transfer between the solid, liquid, and gas phases in homogenous porous media with constant uniform vertical water flow, heat transport is described by [3,19,36,38]:

$$\frac{\partial T}{\partial t} = \frac{\partial}{\partial x}\left[\kappa_{xx}\frac{\partial T}{\partial x}\right] + \frac{\partial}{\partial z}\left[\kappa_{zz}\frac{\partial T}{\partial z}\right] - \left[V_h\frac{\partial T}{\partial z}\right] \quad (1)$$

where T is temperature (K), t is time (s), z is vertical position (m), and κ_{zz} and κ_{xx} denote the effective thermal diffusivities ($m^2\ s^{-1}$) in the z and x directions, respectively, defined by:

$$\kappa_{zz}(\theta) = \frac{\lambda_0(\theta) + \lambda_{d,L}(q_{w,z})}{C_{bulk}(\theta)}, \quad \kappa_{xx}(\theta) = \frac{\lambda_0(\theta) + \lambda_{d,T}(q_{w,z})}{C_{bulk}(\theta)} \quad (2)$$

where λ_0 is the bulk soil thermal conductivity (W m^{-1} K^{-1}), or the so-called stagnant thermal conductivity. $\lambda_{d,L} = \beta_L C_w q_{w,z}$ and $\lambda_{d,T} = \beta_T C_w q_{w,z}$ denote the

longitudinal and transversal thermal dispersion coefficient, respectively, where β_L and β_T are the longitudinal and transverse heat dispersivity (m), and the water flux density, $q_{w,z}$, is uniform and parallel to the z-axis. Neglecting the heat capacity for air, the soil volumetric heat capacity, C_{bulk} (J m^{-3} K^{-1}), can be described by [10]:

$$C_{bulk} = C_s(1-\phi) + C_w\theta \quad (3)$$

where $C = \rho c$ (J m^{-3} K^{-1}) is the heat capacity and the subscripts bulk, s, and w denote the bulk soil, solid, and water phases, respectively, ρ is the density (kg m^{-3}), c is the specific heat (J kg^{-1} K^{-1}), θ is the volumetric water content (m^3 m^{-3}), and ϕ is the porosity (m^3 m^{-3}). In analogy with solute transport, velocity variations within the pore spaces will cause mixing of pore water and thereby create dispersion-like spreading of the temperature field. By including hydrodynamic dispersion on heat transport, the effective thermal conductivity in the longitudinal direction can be written as [19]:

$$\lambda_{eff,zz} = \lambda_0 + \lambda_{d,L} \quad (4)$$

Because of its order-of-magnitude smaller value, we ignore the effect of transverse dispersion. Although heat mixing occurs through all phases, whereas solute mixing is limited to the water phase, values for heat and solute dispersivities should be related [13]. The bulk soil thermal conductivity is relatively large, thus dispersive effects on λ_{eff} are only expected for large water velocities. Hopmans et al. [19] defined the *KJJ*-number to evaluate the contribution of hydrodynamic thermal dispersion to the effective conductivity term:

$$KJJ = \frac{\lambda_{d,L}}{\lambda_0} \quad (5)$$

At increasing pore-water velocities, hydrodynamic effects may become more important to heat transport, so that the need to include dispersion in the bulk thermal diffusivity will depend on the magnitude of the *KJJ*-number. In their sensitivity analysis, Hopmans et al. [19] showed that no thermal dispersion correction is needed if $KJJ < 1$.

The bulk soil thermal conductivity, λ_0, is a function of mineral type, the geometrical arrangement of various phases, and the water content [14]. Chung and Horton [12] proposed a three-parameter polynomial expression to describe the water content dependence of soil thermal conductivity. However, we found that a linear expression was adequate for the soil moisture range of our experiments, or:

$$\lambda_0 = b_0 + b_1\theta \quad (6)$$

where b_0 and b_1 are empirical constants (W m^{-1} K^{-1}). In Eq. (1), V_h denotes the convective heat pulse velocity:

$$V_h = \frac{C_w q_{w,z}}{C_{bulk}} = \frac{\theta C_w v_w}{C_{bulk}} \quad (7)$$

describing heat flow by the moving liquid phase, relative to the stationary bulk porous medium [33]. The heat velocity, V_h, lags behind the water front velocity v_w, since heat is assumed to be instantaneously transferred between the solid, liquid, and gas phases giving thermal homogeneity.

2.2. Water flow

Steady-state variably-saturated water flow in the z direction is described by the Darcy flux, $q_{w,z}$ (m s^{-1}):

$$q_{w,z} = -K(\theta)\left(\frac{\partial h_m}{\partial z} + 1\right) \quad (8)$$

where $K(h_m)$ is the hydraulic conductivity function (m s^{-1}) and h_m is the soil water matric head (m). The two hydraulic relations, the soil water retention curve, $\theta(h_m)$, and the unsaturated hydraulic conductivity function, $K(\theta)$, that are needed to solve Eq. (8), are here described by the van Genuchten and the van Genuchten–Mualem relationships, respectively [43]:

$$S_e(h_m) = \frac{\theta(h_m) - \theta_r}{\theta_s - \theta_r} = [1 + (\alpha|h_m|)^n]^{-m} \quad (9a)$$

$$K(h) = K_s S_e^{0.5}[1 - (1 - S_e^{1/m})^m]^2 \quad (9b)$$

where S_e is the effective saturation, θ_s and θ_r (m^3 m^{-3}) denote saturated and residual water contents, respectively, α (m^{-1}) and n are empirical constants, $m = 1 - 1/n$, and K_s denotes the saturated hydraulic conductivity (m s^{-1}).

2.3. Solute transport

Assuming single domain transport for a conservative tracer with steady-state water flow, one-dimensional solute transport of our experiments is described by the conventional advection–dispersion equation:

$$\theta\frac{\partial C}{\partial t} = \frac{\partial}{\partial z}\left(\theta D\frac{\partial C}{\partial z}\right) - v_w\frac{\partial \theta C}{\partial z} \quad (10)$$

where C is the solute concentration (kg m^{-3}), D is the effective solute dispersion coefficient (m^2 s^{-1}), and $v_w = q_{w,z}/\theta$ is the average pore-water velocity (m s^{-1}). For unsaturated porous media, hydrodynamic dispersion depends on both the water velocity and the water content [41]. Assuming that molecular diffusion is negligible, the hydrodynamic dispersion coefficient reduces to:

$$D = \alpha_L(\theta)v_w \quad (11)$$

where α_L is the longitudinal solute dispersivity (m). Nützmann et al. [29] examined the dependency of dispersivity on the water content in unsaturated porous

media, and derived a linear relation between dispersivity and relative water velocity fluctuations. Their experimental work demonstrated that the relationship between water velocity variations and water content was well described by a power function, to yield the following relation for solute dispersivity:

$$\alpha_L(\theta) = a_1\theta^{a_2} \quad (12)$$

where a_1 (m) and a_2 are constants, to be determined in this study.

3. Materials and methods

Flow column experiments were performed to examine steady-state flow and transport for a range of water saturation, water velocity, and solute concentration values. A newly-developed multi-functional heat pulse probe (MFHPP) by Mori et al. [25,26] was used to monitor coupled heat, water, and solute transport. Inverse modeling techniques were applied for analysis of the experimental data, allowing simultaneous estimation of soil thermal properties (heat conductivity, heat dispersivity, and heat diffusivity) and solute properties (solute concentration and solute dispersion) that are coupled through the soil water properties of water content and water flux. A summary of this new MFHPP device will be presented, followed by a detailed description of the experimental column design and inverse modeling analysis.

The MFHPP is constructed from six sensors (26 mm long and 1.27-mm O.D. stainless steel needles), which are incorporated into a 27-mm radius probe with approximately 6 mm distance between the sensors (Fig. 1). The six sensors include a single central heater sensor, four thermistor sensors located around the heater, and a four-needle Wenner array. Heat pulse experiments are conducted by generating an 8-s heat pulse at the central heater sensor, corresponding to a heat flux of about 60 W m^{-1}, after which the temperature responses at the surrounding thermistor sensors are measured. A detailed description of the design, manufacturing, and implementation of the MFHPP was presented in [25]. Since the heat dissipation depends on the soil's thermal properties, analysis of the temperature signals provides estimates for the soil's thermal diffusivity and conductivity, water content, and water flux density. Various analytical solutions have been developed for heat pulse analysis (see for example [25,33,45]) to successfully estimate these thermal properties and flow variables. In this study, we take it a step further, and will employ inverse numerical modeling techniques for the simultaneous analysis of coupled flow and transport in an experimental column, as described in detail hereafter.

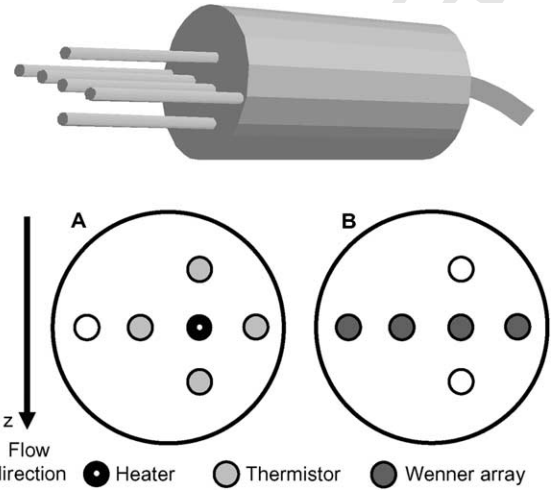

Fig. 1. Schematic of the MFHPP design, with heat pulse measurement using the central heater sensor and the four surrounding thermistors (A) and EC measurements using the horizontal four-needle Wenner array (B).

3.1. Calibration of the MFHPP

Temperature signals were found to be highly sensitive to sensor spacings, so that calibration of each thermistor probe was necessary to achieve satisfactory measurements [22]. Analytical solutions of the heat transport equation were used to calibrate the sensor distance, r, between each thermistor and the heater sensor. The solution describes the temperature increase, ΔT (K), for an infinite line heat source in a homogeneous and isotropic medium after a heat pulse of duration t_0 (s) at a distance r (m) at time $t > t_0$ [6,14,22]:

$$\Delta T(r,t) = \frac{q'}{4\pi C\kappa}\left[Ei\left(\frac{-r^2}{4\kappa(t-t_0)}\right) - Ei\left(\frac{-r^2}{4\kappa t}\right)\right], \quad t > t_0 \quad (13)$$

where q' is the energy input per unit length of heater per unit time (W m^{-1}), and $-Ei(-x)$ denotes the exponential integral operator with argument x [1]. By applying a heat pulse in a media with known heat capacity, C, the distance between the heater and the thermistor, r, can be estimated by fitting the measured temperature response to this analytical solution. Traditionally, an agar–agar solution was used for this calibration since the heat capacity for water is known. Alternatively, in situ calibration was suggested by Mori et al. [25], using a priori information on the heat capacity for the fully saturated media, thereby accounting for changing needle-spacings after insertion into the soil. We followed this approach in our study as well, and repeated it ten times, during the total experimental period, for no-flow conditions at full saturation. Measured temperature signals were fitted to Eq. (13) using Solver, Excel© [46], by fitting the sensor spacing, r, and the thermal diffusivity,

Table 1
Physical properties of washed Tottori Dune sand

Bulk density	ρ_b (kg m^{-3})	1.63
Saturated hydraulic conductivity	K_s (m s^{-1})	2.4×10^{-4}
Saturated water content	θ_s (m^3 m^{-3})	0.371
Residual water content	θ_r (m^3 m^{-3})	0.0535
van Genuchten parameter	α (cm^{-1})	0.0288
van Genuchten parameter	n	12.18
Specific heat	c_s (J kg^{-1} K^{-1})	795.0

κ, using a priori information on the heat capacity, C, for the sand (Table 1). Using 10 datasets, average r-values of each sensor distance and thermal diffusivity were estimated with an average coefficient of variation of 0.34% and 1.30%, respectively. For the total of four MFHPP's, average sensor spacing was 5.91 mm with r-values ranging between 5.52 mm and 6.14 mm.

The four horizontal sensors of the MFHPP (Fig. 1B) were used as a four-electrode Wenner array sensor for bulk soil electrical conductivity (EC_{bulk}) measurements [21,25]. The EC_{bulk} value depends on the solution electrical conductivity, EC_w (mS cm^{-1}), the soil surface conductivity, EC_s (mS cm^{-1}), soil water content, θ, soil bulk density, ρ, temperature, T, and sensor geometry. Assuming the Rhoades et al. [35] relationship to be valid and neglecting the soil surface conductance of the sandy soil, EC_{bulk} is given by:

$$EC_{bulk} = c_1 EC_w \theta^2 + c_2 EC_w \theta \quad (14)$$

where c_1 and c_2 are empirical parameters. Traditionally, the first step in Wenner array calibration is to determine the relationship between measured probe-specific electrical resistance and EC_{bulk} (mS cm^{-1}), using a range of $CaCl_2$ solution concentrations. However, we measured probe-specific electrical resistance directly to determine the relationship between EC_{bulk} and EC_w, both expressed in V V^{-1}, as resistance was measured as the voltage drop relative to the voltage across a reference resistor. For each single probe, EC_{bulk} was measured at various known chloride concentrations for a range of soil water content values (Fig. 2). Subsequently, solute concentration C (mol L^{-1}) was computed from EC_w, using a linear calibration relationship that relates probe-specific electrical resistance to solute concentration. The final result was four different calibration equations for each of the Wenner arrays, with RMSE-values ranging between 21 and 58 V V^{-1}, corresponding with chloride concentration uncertainties of 0.0005–0.0017 mol L^{-1}, respectively. We note that the experimental range of water content values varied between probes. Specifically, MFHPP5 (top of experimental column) and MFHPP2 (bottom of column, Fig. 3) corresponded with the largest and smallest water content ranges, respectively. Rather than having independent water content values available for the calibration, values were estimated from MFHPP measurements for the unsaturated experiments with known chloride concentrations, to be discussed later (Experiments III and IV in Table 2).

3.2. Experimental setup

Steady-state water flow experiments were conducted in a 7.94-cm inner diameter and 30 cm long Plexiglas column packed with 28 cm of Tottori Dune sand (Fig. 3). This Tottori Dune sand was extensively studied in previous investigations [21,25,26], and was selected for this study since its unsaturated hydraulic properties allowed for a relatively large range of measurable water flux density values across a wide water content range. The sand was carefully washed before use with a detergent solution to remove fine clay and silt materials that could potentially clog the porous membrane at the bottom of the column. The retention and unsaturated conductivity characteristics of the washed sand were measured using multi-step outflow experiments, independently [25], whereas the saturated hydraulic conductivity was determined from constant head permeameter measurements. Optimized van Genuchten parameters, as defined in Eqs. (9), were estimated using the SFOPT code [42]. Optimized hydraulic parameters along with the measured saturated hydraulic conductivity are presented in Table 1, whereas the combined soil hydraulic functions are shown in Fig. 4A. The specific heat of the sand, c_s (Table 1), was measured by differential scanning calorimetry as described in [25]. Prior to the flow experiments, the sand was dry-packed in the column at a bulk density of 1.63 g cm^{-3} to a total height of 28 cm. The same sand pack was used for all presented experiments to eliminate differences due to changing heterogeneities. In order to attain full initial saturation prior to each experiment, the sand column was flushed with several pore volumes of CO_2 before saturation from below with de-aired water.

Flow through the sand column was controlled through application of a range of steady-state water flux values, $q_{w,z}$, between 0 and 17.84 m d^{-1}, with corresponding variable suctions at the bottom boundary. Assuming spatial uniformity, these steady-state water fluxes were achieved by an artificial 12-needle rainmaking device. A microtube pump (Masterflex L/S variable-speed digital drives, Cole-Parmer Instrument Company, Vernon Hills, IL) provided for the necessary flow, whereas a six-piece manifold (Fig. 3) connecting to 12 syringe needles provided for a uniform water-sprinkling application to the sand surface. The bottom of the sand column included a metal screen, on which a 20-μm porous nylon membrane (Osmonics R22SP14225, GE Osmonics Labstore, Minnetonka, MN) was glued, with a protective wet strength filter (Whatman Qualitative Wetstrength Filter Paper 114, Whatman Inc., Clifton,

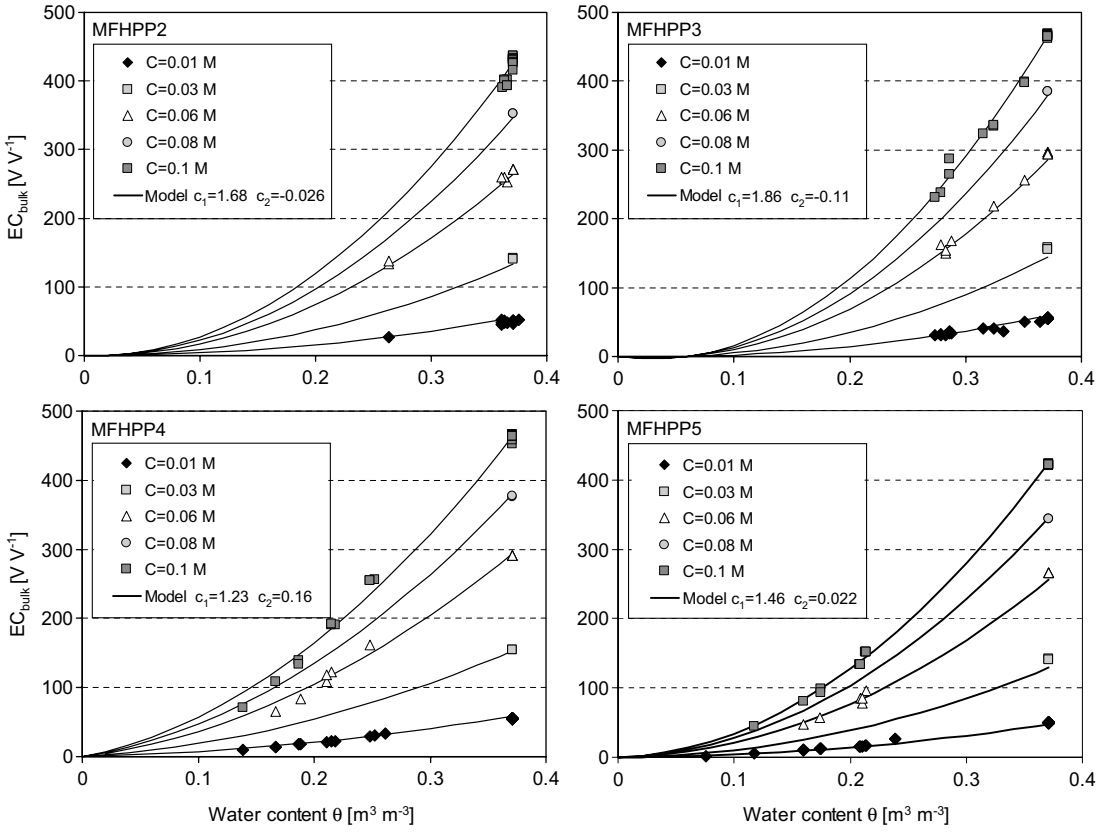

Fig. 2. Calibration of the four-needle Wenner array for the four MFHPPs measuring EC_{bulk} as a function of water content and solute concentration. The model given in Eq. (14) was fitted to the data for each probe with the parameter values c_1 and c_2.

NJ) in between the screen and the nylon. The membrane assured hydraulic continuity between the column and the drainage outlet. The magnitude of the applied boundary suction was controlled by adjusting the outflow height of a tube connected to the bottom outlet.

Tracer solutions were mixed prior to the experiments by adding $CaCl_2$ to distilled water, achieving a range of concentrations of 0.01, 0.03, 0.06, 0.08, and 0.1 mol L^{-1}. The tracer solutions were allowed to equilibrate with the temperature of the laboratory, which was maintained constant within the interval of 18–20 °C. The column was covered with a black fabric to protect it from light, thereby minimizing bacterial growth in the sand.

The various column experiments were monitored with four MFHPP's and four miniature tensiometers (Fig. 3). All instruments were inserted into the Plexiglas column before packing the sand to ensure good and evenly contact. The MFHPP's were inserted such that the four-needle Wenner array was positioned horizontally. The vertical distance between the MFHPP's was 6 cm, with an offset of a 60° angle in between, to minimize flow disturbance along the vertical direction. A CR10 data logger and three AM416 multiplexers (Campbell Scientific) were used to control operation of the MFHPP's, with separate datalogger programs for the temperature and EC measurements. A series of heat pulse measurements was repeated every 15 min. Each 8-s heat pulse was followed by a 120-s period of temperature measurements at the four thermistor sensors. Immediately before the heating, the background temperature of each thermistor sensor was measured and used for calculating the exact temperature increase at each sensor. Separately, during the tracer experiments, EC_{bulk} was measured continuously at each MFHPP with a time resolution of 10 s.

The soil water matrix potential was measured with miniature tensiometers with a 1 cm long and 0.635-cm O.D. ceramic cup [15]. Four tensiometers were inserted approximately 2 cm into the column, at the same depth as the MFHPP's. For the top and bottom MFHPP's, the tensiometers were positioned at an 180° angle with the MFHPP, whereas for the two middle MFHPP's, their angle with the tensiometers was 150° (Fig. 3). The tensiometers were read every 10 s by 1-psi transducers using a separate CR21X datalogger (Campbell Scientific). However, as also pointed out in [25], θ values are extremely sensitive to small measurement errors in h_m for this coarse-textured sandy material (see Fig. 4A). Therefore, we could not use the tensiometric data in the optimizations.

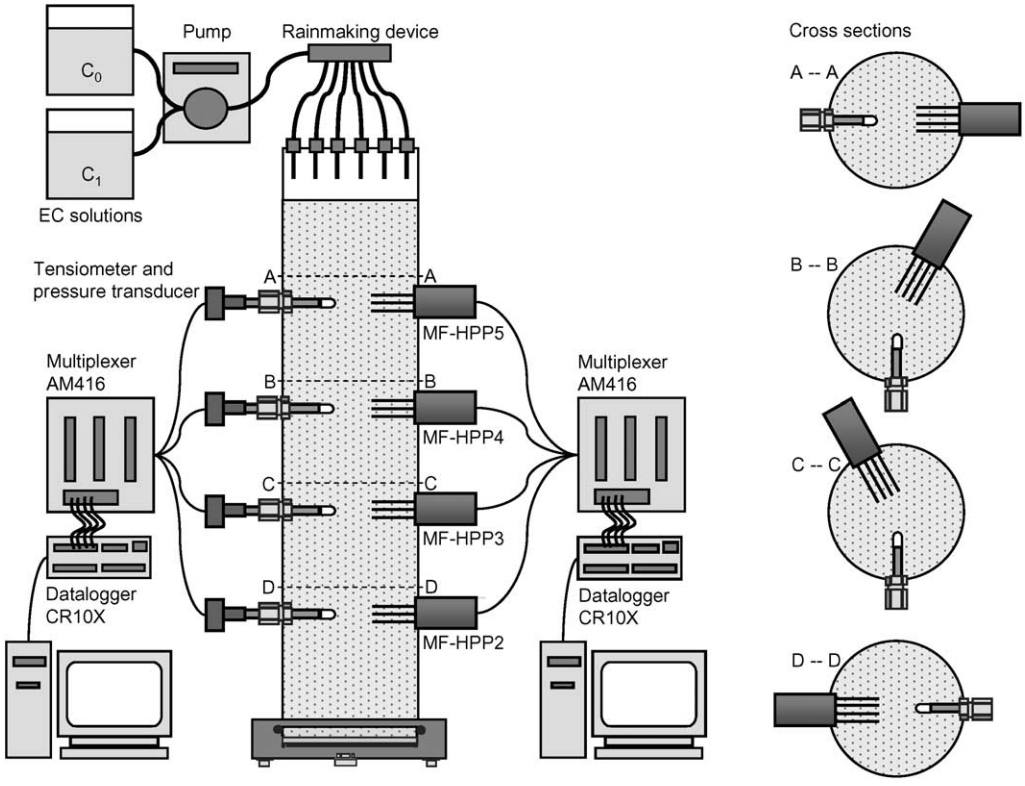

Fig. 3. Schematic of the experimental flow column. The relative positions of the MFHPP's and tensiometers are presented in the cross-sections (right): A–A at 4 cm depth, B–B at 10 cm depth, C–C at 16 cm depth, and D–D at 22 cm depth.

Table 2
Flux and suction boundary values for the saturated and unsaturated experiments

Experiment	Flux Q (mL min^{-1})	Velocity $q_{w,z}$ (m d^{-1})	Boundary pressure h (m)	C_1 (mol L^{-1})	C_2 (mol L^{-1})
I. Saturated with no flow	0.0	0.0	–	–	–
II. Saturated with flow	63	17.84	0.0	0.1	0.01
	46	13.39	0.07	0.01	0.1
	32	9.37	0.14	0.01	0.1
	15	4.37	0.265	0.01	0.1
	3.3	1.05	0.21	0.01	0.1
III. Unsaturated with no flow	0.0	0.0	−0.2	–	–
IV. Unsaturated with flow	20	6.25	−0.2	0.1	0.01
	10	3.12	−0.2	0.1	0.01
	5	1.56	−0.2	0.1	0.06
	2.5	0.78	−0.2	0.06	0.01
	0.6	0.19	−0.2	0.1	0.01

Several tracer experiments were performed for each flow experiment; however the ones used for the inverse modeling are presented with initial concentration C_1 and pulse concentration C_2.

3.3. Experimental matrix

Four different categories of experiments were conducted on the sand column: I. Saturated experiments without flow; II. Saturated experiments with steady-state flow; III. Unsaturated experiments without flow; and IV. Unsaturated experiments with steady-state flow (Table 2). Five different saturated flow experiments were conducted, at which the outflow tube was adjusted to maintain full saturation of the sand column, while preventing water ponding. Also five different unsaturated steady-state flow experiments were performed, all with a constant suction of 20 cm at the lower boundary. For these experiments, the sand was at near-saturation at the bottom of the column and water content decreased upwards with values being a function of the ap-

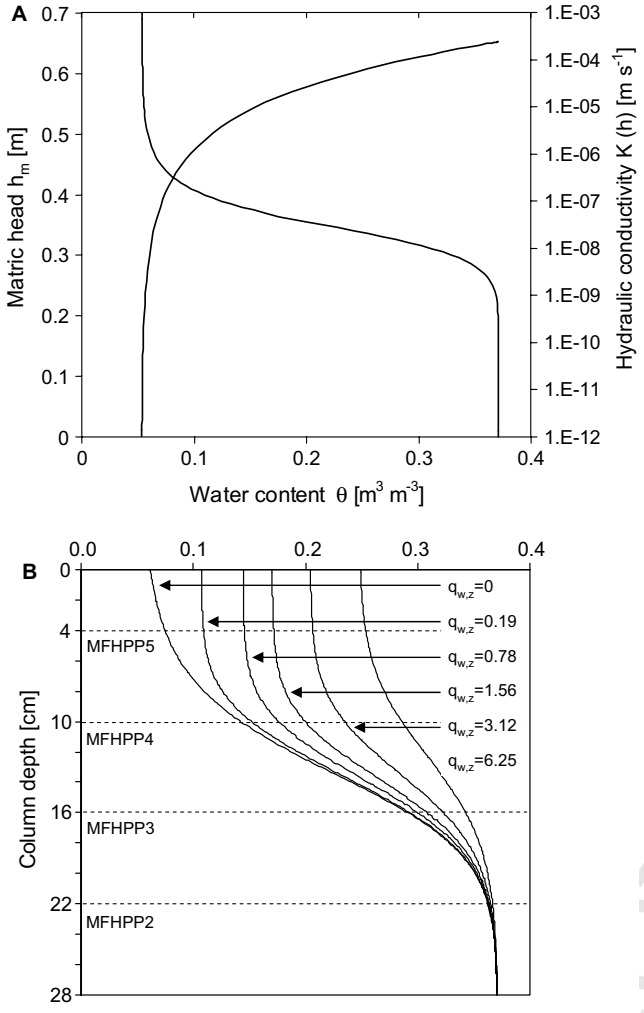

Fig. 4. (A) Retention curve and hydraulic conductivity function measured for the Tottori Dune sand by multi-step outflow experiment. (B) Calculated steady-state distributions of the volumetric water content in the 28 cm sand column for the different infiltration rates $q_{w,z}$ (Table 2). The calculations are based on measured soil hydraulic characteristics (Table 1) and a lower boundary suction of −20 cm. The four MFHPPs were located at 4, 10, 16, and 22 cm depth.

plied flux. The various water content profiles are presented in Fig. 4B, using the soil hydraulic function parameters of Table 1.

Heat pulse measurements were conducted for each single experiment for estimation of thermal and hydraulic properties with a minimum of two measurements for each flow condition and solute concentration. Tracer experiments were conducted for each of the flow experiments by applying $CaCl_2$ as solute tracer using different combinations of the five tracer solutions. The tracer experiments were performed after initial establishment of a constant initial solute concentration, C_1 across the column, switching instantaneously to the invading solution (C_2) at time $t = 0$, while maintaining the same flow rate. This was achieved by connecting two containers with their respective concentrations to the same pump, and simply changing from one to the other concentration by turning a valve (Fig. 3). The transport of the solutes was measured with the four MFHPP's providing tracer breakthrough curves at their four locations in the column. For each flow condition, a minimum of three tracer experiments were conducted by using different combinations of the five tracer solutions. The experiments used for the inverse modeling are listed in Table 2.

3.4. Inverse modeling

Inverse modeling techniques has successfully been applied for a wide range of vadose zone problems [20]. Heat pulse signals have traditionally been analyzed using analytical solutions, both without and with convective heat transport [25,26,33,45]. The opportunities of using inverse modeling techniques for heat pulse analysis were described by Hopmans et al. [19]. Most importantly, inverse modeling allows for the simultaneous estimation of coupled flow and transport parameters. Furthermore, both the number and the type of measurements to be included in the optimization can be varied.

We used the HYDRUS-2D finite element code by Šimůnek et al. [36] for analysis of the MFHPP experiments. The code solves simultaneously water flow with heat and solute transport in two spatial dimensions (x and z). The code solves numerically Richards' equation for saturated–unsaturated water flow and convection–dispersion equations for heat and solute transport. It considers heat transport by conduction, convection, and dispersion, and solute transport by Fickian-based advection–dispersion. HYDRUS-2D uses the Levenberg–Marquardt (LM) algorithm for parameter optimization by inverse modeling. The experiments were simulated for a 3.97 cm (horizontal) by 28 cm (vertical) transport domain, corresponding to the radius and the height of the sand column. A finite element grid was generated so that nodes were positioned at exact locations of the thermistor and EC probe for all four MFHPP's. For the purpose of the numerical analysis, all sensors were assumed to extend infinitely in the y direction, perpendicular to the x–z plane of the simulated domain, thereby ignoring possible three-dimensional effects. The simulated x–z domain consisted of 9855 elements, with a fine nodal spacing of 0.34 mm near the sensor needles, increasing to a coarser resolution of 4.59 mm near the domain boundaries. Depending on the type of experiment, top and bottom flow boundary conditions were defined by water potential or constant flux values and solute transport by a third-type boundary condition. A zero-order source term was added to Eq. (1), defining a non-zero heating rate for the nodes representing the heater needles equal to the specific heat flux measured in the experiment. On all lateral boundaries of the sand domain, a zero water, solute and heat flux was defined. Thermal properties

were defined as presented in Eqs. (12), (3), and (6), and hydraulic properties as in Eq. (9). Although we will demonstrate that θ_r can be estimated concurrent with all other soil hydraulic parameters, we chose to fix it to the independently-estimated value of 0.0535 (Table 1) for most optimizations, since it will generally lead to more unique solutions. Temperature effects on soil hydraulic properties [17] and thermal properties [18] were ignored. Moreover, distillation effects causing enhanced heat transport by latent heat through vaporization and subsequent condensation [9] was not considered at this time. The dependency of EC_{bulk} on solute concentration and water content was included in the model by incorporating the four calibration equations found for each single Wenner array.

For the heat pulse experiments, the objective function Φ to be minimized during the parameter estimation was defined as follows

$$\Phi(\mathbf{p}_{HP}) = W_1 \sum_{i=1}^{N_1} [T^*(\mathbf{x}, t_i) - T(\mathbf{x}, t_i, \mathbf{p}_{HP})]^2 \quad (15)$$

where the right hand size represents the residuals between measured temperatures, T^*, and corresponding predicted temperatures, T. The vector $\mathbf{x}$ denotes the spatial coordinate of each measurement i, N_1 the total number of temperature measurements, W_1 is the weight associated with a particular measurement data point, and the vector $\mathbf{p}_{HP}$ contains the optimized parameters. Two different optimization techniques were applied depending on whether the temperature signals from a single MFHPP or from all four MFHPP's were used to optimize parameters. The number and type of optimized parameters depend on experiment type (Table 3). For the single MFHPP optimizations, the objective function contained temperature data (total of 444) for each of the four thermistors sensors, with measurements each second for a duration of 120 s after heating started. Improved fits to the temperature response data were achieved by introducing a value of 5 to the weighting factor (W_1) of the 16 measurements around the temperature peak. For the saturated experiments, $\mathbf{p}_{HP}$ included the bulk soil volumetric heat capacity, C_{bulk}, and thermal conductivity, λ_0 and also water flux density, $q_{w,z}$, and heat dispersivity, β_L, for the flow experiments. For the unsaturated experiments, the parameter optimization vector $\mathbf{p}_{HP}$ was extended to also include volumetric water content, θ (for the no-flow experiments optimized through C_{bulk}). For the multiple probe optimizations, the objective function included data from all four MFHPP's (in total 1776 data points) with the same weights provided as for single MFHPP optimization. Since the multiple probe optimizations provided column-average parameter values, the $\mathbf{p}_{HP}$ for the unsaturated experiments included functional relationships for thermal conductivity (b_0 and b_1) and unsaturated hydraulic properties functions (α, n, K_s, and θ_r) (Table 3).

For the tracer experiments, the objective function to be minimized was defined by

$$\Phi(\mathbf{p}_{EC}) = W_2 \sum_{i=1}^{N_2} [EC^*_{bulk}(\mathbf{x}, t_i) - EC_{bulk}(\mathbf{x}, t_i, \mathbf{p}_{EC})]^2 \quad (16)$$

where EC^*_{bulk} and EC_{bulk} denote the measured and predicted bulk soil EC, respectively, N_2 defines the number of EC measurements, W_2 is the weight associated with a particular measurement data point, and $\mathbf{p}_{EC}$ contains the optimized parameters. For both saturated and unsaturated experiments, the objective function contained EC measurements from all four MFHPPs. The number and type of optimized parameters were however different for the two experimental groups (Table 3). For saturated flow, optimized parameters included water flux density, $q_{w,z}$, and solute dispersivity, α_L. For the unsaturated tracer experiments, $\mathbf{p}_{EC}$ contained the functional description of the solute dispersivity (i.e. parameters a_1 and a_2 as defined in Eq. (12)), the hydraulic properties (α, n, and K_s) and the water flux density, $q_{w,z}$.

Table 3
Optimized parameters and variables for options A, B, C, and D: soil volumetric heat capacity, C_{bulk}; thermal conductivity, λ_0; thermal conductivity parameters b_0 and b_1, water flux, $q_{w,z}$; water content, θ; residual water content, θ_r; retention parameters α and n; saturated hydraulic conductivity K_s; thermal dispersivity, β_L; solute dispersivity, α_L; solute dispersivity parameters a_1 and a_2

Experiment	Saturated with no flow	Saturated with flow	Unsaturated with no flow	Unsaturated with flow
A. Heat pulse from single MFHPP	λ_0 C_{bulk}	λ_0 β_L $q_{w,z}$	λ_0 θ	λ_0 β_L $q_{w,z}$ θ
B. Heat pulse from multiple MFHPP's	λ_0 C_{bulk}	λ_0 $q_{w,z}$	b_0 b_1 α n θ_r	b_0 b_1 α n θ_r K_s $q_{w,z}$
C. Solute from multiple MFHPP's	–	α_L $q_{w,z}$	–	α_1 α_2 α n K_s $q_{w,z}$
D. Heat pulse and solute from multiple MFHPP's	–	λ_0 α_L $q_{w,z}$	–	b_0 b_1 α_1 α_2 α n K_s $q_{w,z}$

Finally a coupling of both heat pulse and EC_{bulk} data was tested by combining Eqs. (15) and (16) into a single objective function to simultaneously estimate all flow and transport parameters and variables of Table 3. The objective function included both temperature and EC_{bulk} measurements for all four MFHPP's. Internal weighting was accomplished by including the number of measurements and variance in W_1 and W_2, thereby achieving equal weight between the different data types, as recommended in [20].

4. Results and discussion

Measured temperature differences of all four thermistors for each MFHPP device were used to estimate both soil thermal and hydraulic parameters. As an example, we present a comparison of measured with optimized temperature signals for unsaturated experiments at zero-flow and at steady-state flow of $q_{w,z} = 6.25\ m\ d^{-1}$ in Fig. 5. In the absence of water flow, heat is transported by conduction only, resulting in symmetrical spreading of the heat pulse around the heater needle to all four surrounding thermistors equally, with slight variations caused by variable sensor spacing and soil heterogeneities. In contrast, asymmetrical temperature responses occur for the steady-state flow water experiments with heat convection, resulting in temperature differences between the upstream, downstream, and transverse thermistor locations [19]. However, in either case, the temperature response will increase with decreasing soil water content. EC measurements were analyzed to estimate solute dispersivity and water flux, with and without simultaneous temperature response measurements. Hereafter, we will discuss the optimization results of four different options, A through D, of which the experimental settings are listed in the first column of Table 3.

4.1. Thermal and hydraulic properties from single MFHPP measurements

The single probe optimizations of both unsaturated zero-flow and steady-state experiments included estimations of the volumetric water content, θ. These estimated water content values are compared with the corresponding simulated water content values (from hydraulic parameters, Table 1) in Fig. 6, with a RMSE of $0.019\ m^3\ m^{-3}$. The relative water content errors, as defined by $(\theta_{est} - \theta_{true})/\theta_{true}$, were on average smaller than ±10% between all MFHPP's, and were unbiased. In our simulations with HYDRUS-2D, temperature data for all four thermistors were included to estimate average water content. Yet, significant differences in water contents with vertical position might occur, because of the large sensitivity of the sand soil moisture to the matric head (Fig. 4A). In part, this explains slightly larger errors in the intermediate water content range of Fig. 6, as differences in θ between the upstream and downstream thermistors could be as large as $0.03\ m^3\ m^{-3}$ for some flow experiments.

Mori et al. [25,26] also used the MFHPP technique for water content estimation and applied the analytical solution of heat transport equation using the horizontal thermistor only, assuming that this thermistor is least affected by convective transport. Although they found excellent agreement for water fluxes smaller than

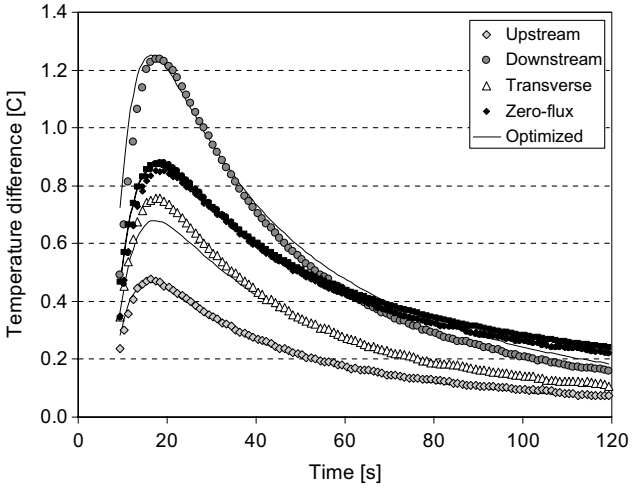

Fig. 5. Example of measured and estimated temperature responses at upstream, downstream, and transverse thermistor sensors for unsaturated experiments with no flow ($\theta = 0.147$; $q_{wz} = 0\ m\ d^{-1}$) and steady-state flow ($\theta = 0.213$; $q_{wz} = 6.25\ m\ d^{-1}$).

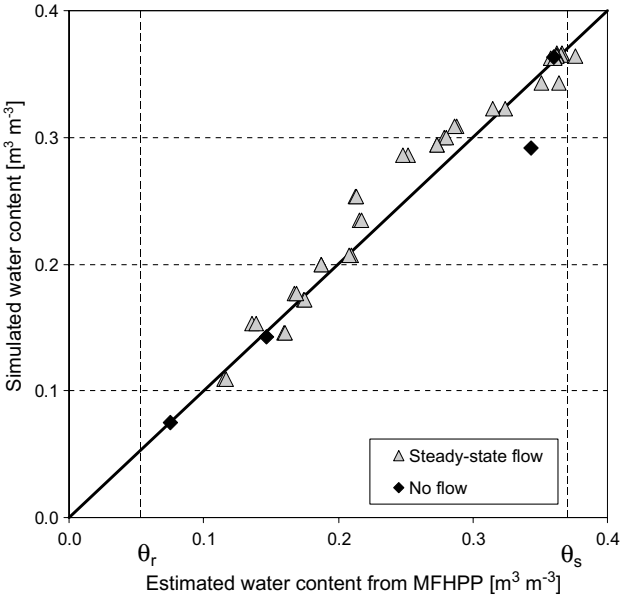

Fig. 6. Volumetric water contents estimated from single MFHPP optimizations (option A) compared with the simulated water contents (calculated from retention characteristics in Table 2).

0.5 m d^{-1} (RMSE of 0.0056 m^3 m^{-3}), estimated water content values were significantly overestimated for higher water fluxes, as their analytical solution neglected convective heat transport. Also Kluitenberg and Heitman [23] examined the influence of water flux density and thermistor orientation on water content estimation errors using analytical solutions, and concluded that water content errors increased with increasing water flux.

Simultaneously with soil water content, the soil thermal conductivity, λ_0, was estimated from both saturated and unsaturated experiments for both zero-flux and a series of steady-state flow conditions (Table 2). Estimated thermal conductivities for all experiments combined are presented in Fig. 7 as a function of the soil water content, as estimated from the MFHPP measurements. The linear relation of Eq. (6) was fitted to the data, thereby characterizing the water content dependency of thermal conductivity of the Tottori sand as a function of water content, resulting in values of b_0 = 1.13 and b_1 = 1.68 (W m^{-1} K^{-1}), with a RMSE value of 0.003 W m^{-1} K^{-1}. Our data compared remarkably well with the independent sandy soil data of Hopmans and Dane [17], as was also found from previous work by Mori et al. [25,26], who used the MFHPP technique in combination with analytical solutions. Yet, Mori et al. [26] concluded that the MFHPP measurements overestimated the thermal conductivity for water fluxes larger than 2 m d^{-1}. Their analytical solutions necessitated the fitting to the horizontal thermistor measurements only, thereby largely neglecting the influence of convection. In our case, we used all four thermistors simultaneously in the numerical model, allowing for the coupling between thermal transport and water flow. Therefore, the final outcome in Fig. 7 was not affected by the magnitude of the water flux density. Note that we do not attempt to estimate the thermal conductivities for water content values smaller than about 0.1, since this is below our measurement range.

In addition to water content and thermal properties, the single probe optimizations also yielded estimated water flux densities. Estimated water fluxes are compared with the true fluxes, as computed from volumetric drainage flow rates in Fig. 8. More accurate flux estimates were generally obtained for the unsaturated flow experiments (RMSE of 0.49 m d^{-1}) as compared to the saturated experiments (RMSE of 1.94 m d^{-1}), with the mostly higher flow rates. Relative flux errors, as defined by $(q_{wz,est} - q_{wz,true})/q_{wz,true}$, were calculated for each MFHPP for both the saturated and unsaturated flow. For the saturated flow experiments, water fluxes were generally underestimated, with relative errors between 10% and 20%; however, the errors of MFHPP2 at the column bottom were significantly larger (13–26%). For the unsaturated steady-state flow experiments, the MFHPP optimizations generally underestimated the flow at high water fluxes as well, but relative errors were positive for the low flow rate experiments, with MFHPP2 showing the largest relative errors. In contrast to the flux rate-independent errors for the saturated experiments, the relative flux error increased as water flux decreased for the unsaturated experiments. We note that the lower water fluxes correspond with smaller water content values in the column (Fig. 4B).

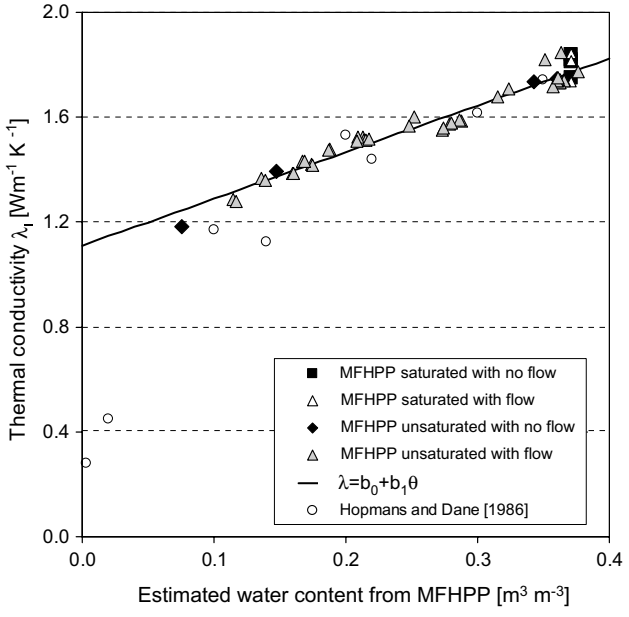

Fig. 7. Thermal conductivities estimated from single MFHPP optimizations (option A) as a function of the estimated water content from single MFHPP.

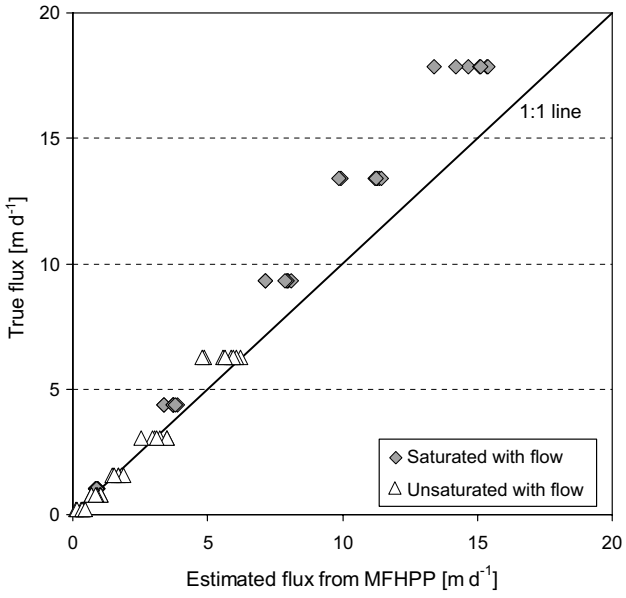

Fig. 8. Water fluxes estimated from single MFHPP optimizations (option A) compared with the true fluxes applied as top boundary.

Various other studies also concluded that HPP measurements underestimated water flux at high flow rates [19,25,26,33]. However, both studies of Mori et al. [25,26] point out the difficulty in estimating water fluxes if values are smaller than 0.1 m d^{-1}. It was suggested that the limitation of the MFHPP in the low water flux range is controlled by the temperature resolution of the thermistors (0.01 °C).

The underestimation in the high water flux range was attributed by Hopmans et al. [19] to thermal dispersion. Therefore, in the single probe optimizations, we included the longitudinal heat dispersivity (Eq. (4)), β_L, as an additional estimation parameter in both saturated and unsaturated flow experiments. However, the estimated values were generally small, with average values of 0.004 cm (CV = 1.7×10^{-5}) for saturated experiments and 0.006 cm (CV = 9.75×10^{-5}) for unsaturated experiments. These low values suggest that thermal dispersion is not important in our sand, as is to be expected with average *KJJ*-numbers (Eq. (5)) of 0.01 (CV = 2.3×10^{-4}) and 0.008 (CV = 3.1×10^{-4}) for the saturated and unsaturated experiments, respectively. These values are considerably lower than the threshold value of *KJJ* = 1, for which heat dispersion becomes important [19]. Optimizations that excluded thermal dispersion confirmed that this process was not important for our experiments. Moreover, it is expected that dispersivity values will be small if determined from measurements over such small travel distances (~6 mm) between the heater and the upstream and downstream thermistors.

4.2. Thermal and hydraulic properties from multiple MFHPP measurements

For the multiple probe optimizations the temperature differences for all four MFHPP's, for a total of 16 temperature signals, were included into the objective function. For the saturated experiments, this resulted in column-average values for the saturated thermal conductivity and water flux (Table 3). For the unsaturated experiments, the simultaneous use of all MFHPP data provided optimized parameter values for the water content dependent thermal conductivity function in Eq. (6), α, n and K_s values of the soil hydraulic functions (Eq. (9)), and the water flux density, $q_{w,z}$ (Table 3).

The results of the multiple probe optimizations is presented in Table 4 and Fig. 9, whereas the optimized water flux density values are included in Fig. 11. For the saturated conditions, the optimized thermal conductivity and water flux values agreed with corresponding average values for the single probe optimizations. For the unsaturated experiments, each steady-state flow creates water content profiles that are determined by water flux density (Fig. 4B), so that optimization results apply to each specific water content range only. Specifically, at high water fluxes, the water content range is limited. For

Table 4
Option B. Optimized thermal and hydraulic properties for multiple probe optimizations of unsaturated experiments

Saturated experiments	Thermal properties	Hydraulic properties	Unsaturated experiments	Thermal properties		Hydraulic properties				
	λ_0 (W m^{-1} K^{-1})	$q_{w,z}$ (m d^{-1})		h_0 (W m^{-1} K^{-1})	h_1 (W m^{-1} K^{-1})	α (cm^{-1})	n	θ_r (m^3 m^{-3})	K_s (m s^{-1})	$q_{w,z}$ (m d^{-1})
Single probe/multi-step outflow	1.80	–		1.134	1.68	0.0288	12.18	0.0535	2.4E−4	–
$q_{w,z}$ = 17.84 m d^{-1}	1.82	15.05	$q_{w,z}$ = 6.25 m d^{-1}	0.822	2.77	0.0292	17.93	0.00024	2.5E−4	NO
$q_{w,z}$ = 13.39 m d^{-1}	1.75	10.52	$q_{w,z}$ = 3.12 m d^{-1}	1.11	1.97	0.0311	19.93	0.0015	1.8E−4	3.27
$q_{w,z}$ = 9.37 m d^{-1}	1.78	7.79	$q_{w,z}$ = 1.56 m d^{-1}	1.16	1.63	0.0305	13.32	0.00018	1.6E−4	1.70
$q_{w,z}$ = 4.37 m d^{-1}	1.80	3.72	$q_{w,z}$ = 0.78 m d^{-1}	1.15	1.63	0.0301	13.04	0.0395	1.9E−4	0.94
$q_{w,z}$ = 1.05 m d^{-1}	1.79	0.90	$q_{w,z}$ = 0.19 m d^{-1}	1.04	3.28	0.0290	13.55	0.024	1.4E−4	0.19
$q_{w,z}$ = 0 m d^{-1}	1.80	–	$q_{w,z}$ = 0 m d^{-1}	1.05	1.91	0.0278	19.23	0.0650	–	–

For comparison, thermal properties from single probe optimization and hydraulic properties from multi-step outflow experiments are included in the first row.
NO: not optimized. Solutions did not converge.

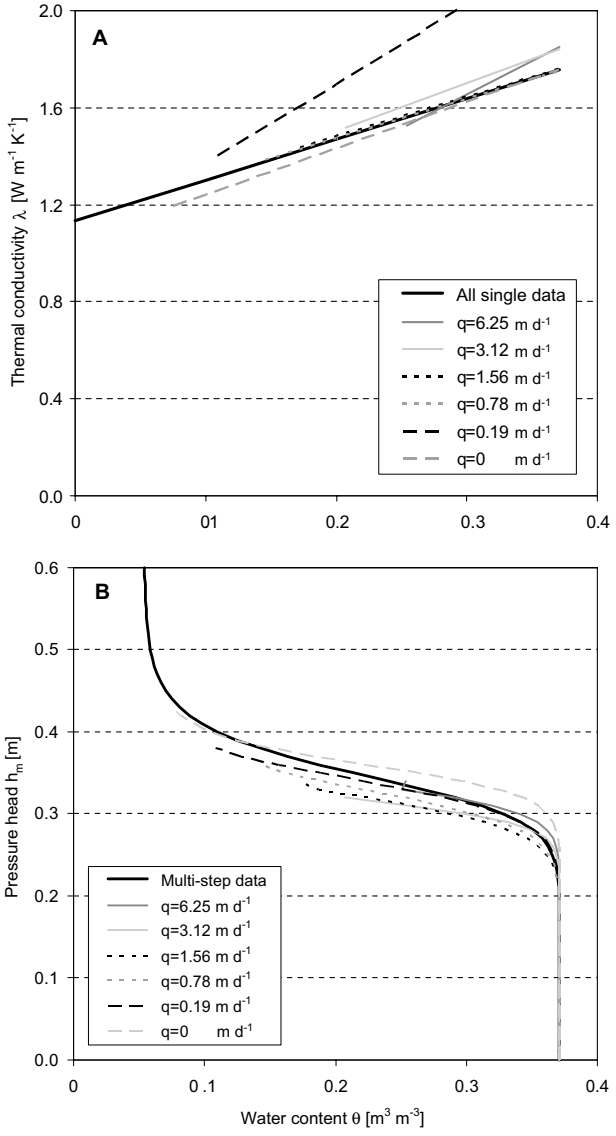

Fig. 9. Thermal and hydraulic properties from multiple MFHPP optimization of unsaturated experiments (option B). Based on estimated parameters (Table 4) the thermal conductivity function (A) and retention curve (B) is presented for the water content range applicable for each flow rate.

example, for a steady-state flux of $q_{w,z} = 6.25$ m d^{-1}, the experimental water content range is limited to only that between 0.371 and 0.25. Alternatively, the experimental water content range is between 0.11 and 0.37 m^3 m^{-3} for the applied steady-state flux of 0.19 m d^{-1}, thereby providing a much complete and accurate description of the functional relationship across the entire water content range.

The optimized thermal conductivity parameters for the unsaturated experiments are compared with the values found from the single MFHPP optimization (option A) in Table 4 and Fig. 9A. Although, the multiple probe optimizations agree well with the single probe results, the case with $q_{w,z} = 0.19$ m d^{-1} (black dashed line in Fig. 9A) is an exception. Table 4 and Fig 9B presents the optimized soil water retention parameters for the different steady flux rates, and compare them with independent values, as obtained from the multi-step outflow experiments. As expected, the most accurate optimized retention parameters across the experimental water content range were determined from the low water flux experiments. Although not shown, when optimizations were carried out with a fixed residual water content value of $\theta_r = 0.0535$ m^3 m^{-3}, a much improved description of the retention curve for the high flux steady-state experiments was obtained.

Using multiple datasets provided several advantages for characterization of thermal and hydraulic properties. First, by selecting the most optimal experimental conditions, a single experiment, with MFHPP's installed at different depths that combined cover a wide range of water contents, may provide sufficient information for a complete description of the soil thermal conductivity and soil hydraulic functions. In contrast, to obtain the same information from a single probe, many measurements at different water contents would be necessary. Second, the single probe optimizations would require soil water potential measurements at the MFHPP locations, to obtain soil water retention curve parameters. The multiple probe approach only needs measured values for the bottom boundary head ($h_m = -20$ cm for our experiments) for successful optimization.

4.3. Tracer experiments

For the tracer experiments, the objective function consists of EC_{bulk} values, as measured by the four-electrode Wenner array of the four MFHPP's for each of the 10 steady-state water fluxes (duplicate for each flux density). Since the EC_{bulk} contains information on both solute concentration and volumetric water content, breakthrough measurements were used to simultaneously estimate both soil hydraulic and solute transport parameters [21,37]. The individual calibration equations of Eq. (14) for each MFHPP were included in the HYDRUS-2D code, so that calculated solute concentrations and water contents could be used to evaluate EC_{bulk}, and then used in the optimization process. The dependency of water content on EC_{bulk} resulted in distinctly different breakthrough curves for both the saturated (Fig. 10A) and unsaturated (Fig. 10B) flow experiments, with EC_{bulk} differences at equal concentrations between probes (such as the offset) attributed to individual calibration equations. When comparing the results, we also notice the slightly larger noise in concentration values for the unsaturated experiments, even though the average velocity was much larger for the saturated experiments. More disturbing are the unstable concentration values found along some of the saturated breakthrough curves at high EC_{bulk} values resulting in

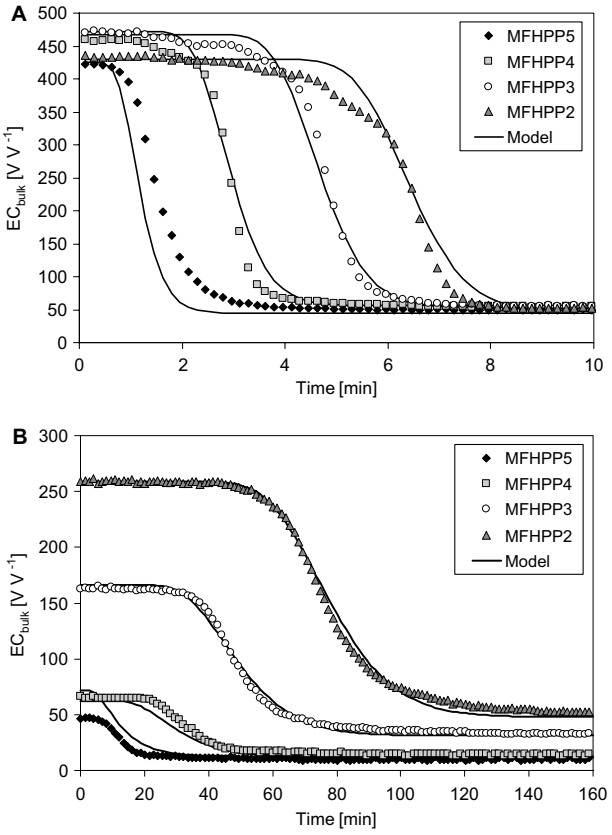

Fig. 10. Example of measured and estimated EC_{bulk} breakthrough curves for (A) saturated flow at $q_{wz} = 17.84$ m d^{-1} and (B) unsaturated flow at $q_{wz} = 0.78$ m d^{-1}. Measured EC_{bulk} is both a function of the probe and the water content, which is described by individual calibration equations.

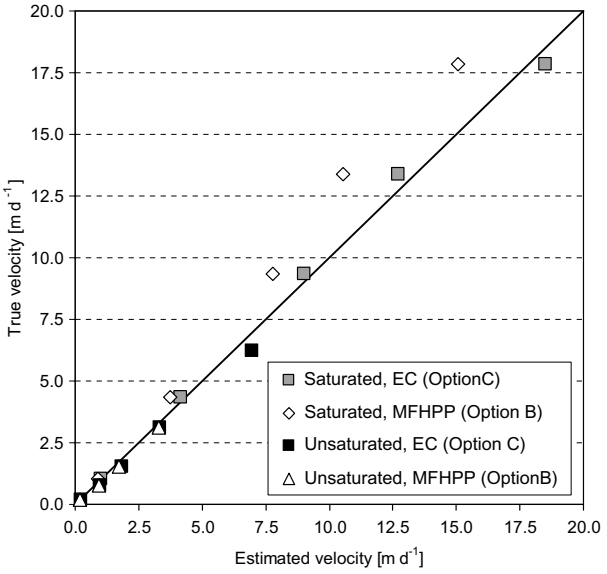

Fig. 11. Water fluxes estimated from multiple probe EC_{bulk} optimizations (option C) compared with the true water fluxes applied as top boundary (values presented in Table 5). Estimated water fluxes from multiple probe heat pulse optimizations (option B, Table 4) are included for comparison.

"bumps" on the breakthrough curves for reasons that are unclear. Alike disturbances in the break through curves were measured consistently for all MFHPP's at EC_{bulk} values larger than about 350 mS cm^{-1}, indicating slightly unstable Wenner array measurements at these high concentrations. Finally, the unsaturated breakthrough curves showed significant tailing, which has been observed in general for unsaturated breakthrough curves (e.g. [31]).

Optimized parameters for the saturated and unsaturated experiments are presented in Table 5. The optimized water flux values are compared in Fig. 11 with the true water fluxes and with those estimated with option B (i.e., multiple MFHPP's heat pulse signals). RMSE values were 0.458 and 0.357 m d^{-1} for the saturated and unsaturated experiments, respectively. Generally, the tracer optimizations gave better flux estimates for the saturated experiments, especially for the high flux experiments for which options A and B underestimated the water flux. This is not surprising as solute breakthrough is largely controlled by convection, especially for the relatively high water fluxes of this experiment. For the unsaturated experiments, very similar optimization results were found for the tracer experiments and the heat pulse experiments.

In addition to water fluxes, solute dispersivity values were also optimized (Table 5). For the saturated experiments, solute dispersivity was optimized directly with estimated values between 0.306 and 0.580 cm. For the unsaturated experiments, the water content dependence of solute dispersivity was optimized through the two parameters α_1 and α_2, as defined in Eq. (12), with the

Table 5
Option C. Optimized solute and hydraulic properties from multiple probe optimizations of saturated and unsaturated tracer experiments

Saturated experiments	Solute properties	Hydraulic properties	Unsaturated experiments	Solute properties		Hydraulic properties			
	α_L (cm)	$q_{w,z}$ (m d^{-1})		α_1 (cm)	α_2	α (cm^{-1})	n	K_s (m s^{-1})	$q_{w,z}$ (m d^{-1})
$q_{w,z} = 17.84$ m d^{-1}	0.580	18.49	$q_{w,z} = 6.25$ m d^{-1}	0.0643	−1.73	0.0287	6.64	3.5E−4	6.94
$q_{w,z} = 13.39$ m d^{-1}	0.360	12.70	$q_{w,z} = 3.12$ m d^{-1}	0.000886	−3.17	0.0293	6.98	2.2E−4	3.33
$q_{w,z} = 9.37$ m d^{-1}	0.312	8.99	$q_{w,z} = 1.56$ m d^{-1}	0.000223	−3.47	0.0321	14.54	1.8E−4	1.84
$q_{w,z} = 4.37$ m d^{-1}	0.306	4.16	$q_{w,z} = 0.78$ m d^{-1}	0.00205	−2.17	0.0327	17.13	0.9E−4	0.97
$q_{w,z} = 1.05$ m d^{-1}	0.480	1.00	$q_{w,z} = 0.19$ m d^{-1}	0.000635	−2.59	0.0308	7.48	2.7E−4	0.21

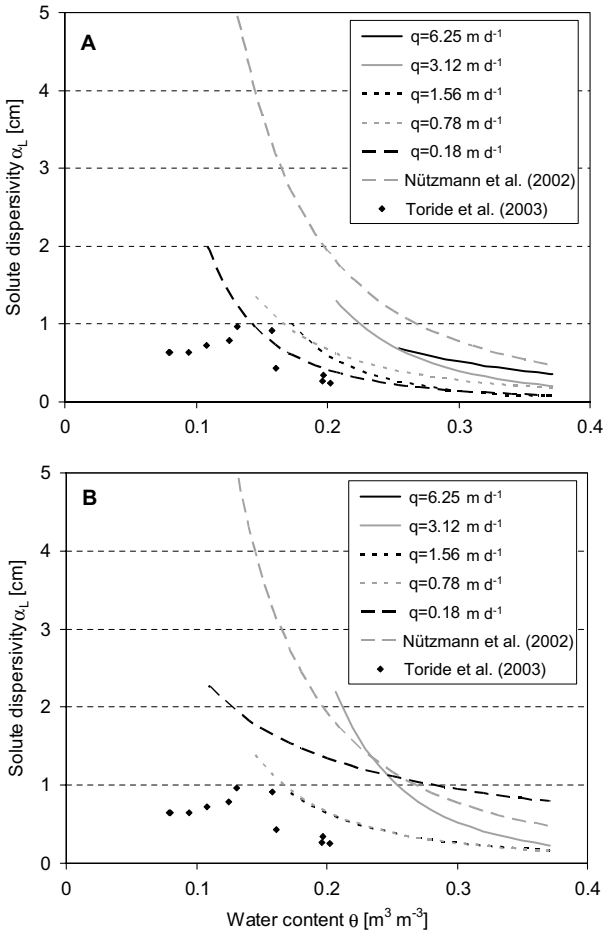

Fig. 12. Solute dispersivity α_L as a function of water content (Eq. (12)) based on estimated parameters α_1 and α_2 from (A) multiple optimization of for unsaturated flow experiments (option C) and (B) multiple optimization of coupled heat and solute flow experiments (option D). Corresponding estimated parameter values are presented in Tables 5 and 6.

parameter values and the functional forms presented in Table 5 and Fig. 12A. As for option B, the most widely applicable results are expected for the lower flux experiments ($q_w = 0.18$ m d^{-1}) for which the water content range was the largest. Interestingly, for these optimizations, our results most closely approach those of Toride et al. [41]. The optimized parameter values compared reasonably well with those found by Nützmann et al. [29] for a coarse-textured sand with $\alpha_1 = 0.0517$ cm and $\alpha_2 = -2.25$ (Fig. 12A).

Also the soil hydraulic property parameters α, n, and K_s were optimized from the unsaturated tracer experiment results, simultaneously with the dispersivity parameters (Table 5). As expected, the best results were obtained for the steady-state flow experiments with the lowest fluxes that correspond with the largest water content range. However, in general we conclude that the EC_{bulk} data alone was less suitable for estimation of the hydraulic properties.

4.4. Coupled water, heat, and solute transport optimizations

As will be demonstrated hereafter, the presented MFHPP technique allows simultaneous measurement of parameters and variables characterizing coupled water, heat, and solute transport. The option B results demonstrated that coupled water flow and heat transport was characterized from optimization of the heat pulse measurements, allowing simultaneous estimation of both thermal and hydraulic properties. Likewise, coupled water flow and solute transport parameters were estimated from the EC_{bulk} measurements, providing information for simultaneous estimation of solute transport and hydraulic properties. In this last section, we will demonstrate that coupled water, heat, and solute processes can be analyzed simultaneously using a combination of temperature and EC_{bulk} measurements in the same objective function.

Optimized parameters for both saturated and unsaturated flow experiments are presented in Table 6. We note that as for option B, the highest flux optimizations did not converge. Several differences were noticed when using coupled heat and solute data for the inverse analysis instead of heat (option B, Table 4) or solute (option C, Table 5) data alone. First, whereas excellent water flux estimates were obtained for saturated flow in option C, the coupled approach estimates were not as good, though closer than the underestimation of option B. This was expected. However, water flux errors resulted in slightly larger estimated values for solute dispersivity (Table 6). For the unsaturated experiments, the differences in flux estimates between options B and C were minor, hence the coupled estimates (option D) were equally accurate. Coupling the temperature with the breakthrough data resulted in an excellent description of the soil water retention characteristics, especially for the low flux density experiments. The improved soil water retention optimization also affected the optimized solute dispersivity functions (compare Fig. 12A and B), because of the influence of water content on EC_{bulk}. However, we note that the same general soil moisture effects on solute dispersivity were determined. Concurrent optimized values for the thermal conductivity parameters were similar or better than using option B, and compared very well with the single MFHPP optimization results of option A.

Although the coupled optimizations were successful in many ways, the corresponding fitting to the solute breakthrough curves was generally disappointing. We believe it to be mostly caused by the relative high uncertainty of the EC_{bulk} measurements. First, as pointed out in Section 3.1, the number of data pairs for the Wenner array calibrations were limited, and was different between probes. Second, we hypothesize that the Wenner array sensor is unstable in the range with the highest

Table 6
Option D. Optimized parameters from coupled heat pulse and tracer experiments for saturated and unsaturated conditions

Saturated experiments	Thermal properties	Solute properties	Hydraulic properties	Unsaturated experiments	Thermal properties		Solute properties		Hydraulic properties			
	λ_0 (W m^{-1} K^{-1})	α_L (cm)	$q_{w,z}$ (m d^{-1})		b_0 (W m^{-1} K^{-1})	b_1 (W m^{-1} K^{-1})	α_1 (cm)	α_2	α (cm^{-1})	n	K_s (m s^{-1})	$q_{w,z}$ (m d^{-1})
$q_{w,z}$ = 17.84 m d^{-1}	1.87	0.688	16.12	$q_{w,z}$ = 6.25 m d^{-1}	NO	NO	NO	NO	NO	NO	NO	NO
$q_{w,z}$ = 13.39 m d^{-1}	1.86	0.633	11.85	$q_{w,z}$ = 3.12 m d^{-1}	1.18	1.75	0.0051	−3.85	0.0308	16.27	2.7E−4	3.41
$q_{w,z}$ = 9.37 m d^{-1}	1.84	0.516	8.33	$q_{w,z}$ = 1.56 m d^{-1}	1.08	1.97	0.018	−2.22	0.0310	14.29	2.4E−4	1.73
$q_{w,z}$ = 4.37 m d^{-1}	1.83	0.434	3.99	$q_{w,z}$ = 0.78 m d^{-1}	1.44	1.60	0.016	−2.31	0.0302	12.97	1.9E−4	0.91
$q_{w,z}$ = 1.05 m d^{-1}	1.79	0.509	0.98	$q_{w,z}$ = 0.19 m d^{-1}	1.07	1.99	0.338	−0.86	0.0298	11.21	3.0E−4	0.25

NO: not optimized. Solutions did not converge.

water content and solute concentration values, corresponding with the largest experimental range of EC_{bulk} values.

5. Summary and conclusions

The new MFHPP technique combined with inverse modeling allowed for simultaneous estimation of coupled thermal, hydraulic, and solute properties. Single probe inverse optimization allowed simultaneous estimation of thermal characteristics, such as thermal conductivity and heat dispersion, soil hydraulic properties, water flux density and volumetric water content. Estimated parameters were generally in good agreement with independently-measured values. Thermal dispersivity was found to be insignificant, confirming that heat dispersion was not important in our experiments. The main advantage of multiple probe optimizations is that the water content dependency of thermal and hydraulic relationships could be determined simultaneously from the coupled column experiments, provided that a wide range in experimental water content values can be achieved.

The Wenner array of the MFHPP provided for bulk soil EC measurements during tracer breakthrough. Since the EC measurements include information on both solute concentration and soil water content, the coupled estimation of solute dispersivity and hydraulic parameters was possible. For the unsaturated tracer experiments, we conclude that the solute dispersivity's dependence on water content was described by a power function. However, we also found that the Wenner array is not performing accurately at full saturation, in the range of high solute concentrations.

The combination of MFHPP measurements with inverse numerical analyses is shown to be a promising method for the simultaneous analysis of coupled water, heat, and solute flow processes in variably-saturated porous media. The probe's ability to simultaneously measure thermal, hydraulic, and solute properties within the same sample volume provides for a new powerful tool for vadose zone monitoring and characterization. Moreover, we show that new insights can be learnt from the analysis of coupled flow and transport measurements. Although the current study examines steady-state flow only, the MFHPP performs equally well for transient flow conditions.

Acknowledgments

The authors wish to thank Dr. Keith Bristow of CSIRO Land and Water, Australia for allowing us to use their prototype of the four-needle heat pulse probe. We also thank Dr. Gerard Kluitenberg for his com-

ments and encouragement. APM acknowledges funding from VILLUM KANN RASMUSSEN and DONG's Jubilæumslegat. YM acknowledges funding from Japan Society for the Promotion of Science (2001–2003). The work was also supported in part by SAHRA (Sustainability of semi-Arid Hydrology and Riparian Areas) under the STC Program of the National Science Foundation, Agreement No. EAR-9876800.

References

[1] Abramovitz M, Stegun I. Handbook of mathematical functions. New York: Dover Publications; 1972 [p. 231].
[2] Basinger JM, Kluitenberg GJ, Ham JM, Frank JM, Barnes PL, Kirkham MB. Laboratory evaluation of the dual-probe heat pulse method for measuring soil water content. Vadose Zone J 2003;2:389–99.
[3] Bear J. Dynamics of fluids in porous media. New York: Elsevier; 1972.
[4] Bilskie JR, Horton R, Bristow KL. Test of a dual-probe heat-pulse method for determining thermal properties of porous materials. Soil Sci 1998;163:346–55.
[5] Bristow KL, Campbell GS, Calissendorff K. Test of a heat-pulse probe for measuring changes in soil water content. Soil Sci Am J 1993;57:930–4.
[6] Bristow KL, Kluitenberg GJ, Horton R. Measurement of soil thermal properties with a dual-probe heat-pulse technique. Soil Sci Soc Am J 1994;58:1288–94.
[7] Bristow KL. Measurement of thermal properties and water content of unsaturated sandy soil using dual-probe heat-pulse probes. Agric Forest Meteorol 1998;89:75–84.
[8] Bristow KL, Kluitenberg GJ, Goding CJ, Fitzgerald TS. A small multi-needle probe for measuring soil thermal properties, water content and electrical conductivity. Comput Electron Agric 2001;31:265–80.
[9] Cass A, Campbell GS, Jones TL. Enhancement of thermal vapor diffusion in soil. Soil Sci Am J 1984;48:25–32.
[10] Campbell GS. Soil physics with BASIC—transport models for soil-plant systems. New York: Elsevier; 1985.
[11] Campbell GS, Calissendorff C, Williams JH. Probe for measuring soil specific heat using a heat-pulse method. Soil Sci Am J 1991;55:291–3.
[12] Chung S-O, Horton R. Soil heat and water flow with a partial surface mulch. Water Resour Res 1987;23:2175–86.
[13] de Marsily G. Quantitative hydrogeology: groundwater hydrology for engineers. San Diego: Academic; 1986.
[14] de Vries DA. Thermal properties of soils. In: van Wijk WR, editor. Physics of plant environment. New York: North-Holland; 1963.
[15] Eching SO, Hopmans JW. Optimization of hydraulic functions from transient outflow and soil water pressure data. Soil Sci Soc Am J 1993;57:1167–75.
[16] Heitman JL, Basinger JM, Kluitenberg GJ, Ham JM, Frank JM, Barnes PL. Field evaluation of the dual-probe heat pulse method for measuring soil water content. Vadose Zone J 2003;2:552–60.
[17] Hopmans JW, Dane JH. Thermal conductivity of two porous media as a function of water content, temperature, and density. Soil Sci 1986;142:187–95.
[18] Hopmans JW, Dane JH. Temperature dependency of soil hydraulic properties. Soil Sci Am J 1986;50:4–9.
[19] Hopmans JW, Šimůnek J, Bristow KL. Indirect estimation of soil thermal properties and water flux using heat pulse probe measurement: geometry and dispersion effects. Water Resour Res 2002;38(1). doi:10.1029/2000WR000071.
[20] Hopmans JW, Šimunek J, Romano N, Durner W. Simultaneous determination of water transmission and retention properties—inverse modeling of transient water flow. In: Topp GC, Dane JH, editors. Methods of soil analysis, Part 4. Physical methods. Soil Science Society of America Book Series, no. 5.
[21] Inoue M, Šimůnek J, Shiozawa S, Hopmans JW. Simultaneous estimation of soil hydraulic and solute transport parameters from transient infiltration experiments. Adv Water Resour 2000;23:677–88.
[22] Kluitenberg GJ, Ham JM, Bristow KL. Error analysis of the heat pulse method for measuring soil volumetric heat capacity. Soil Sci Am J 1993;57:1444–51.
[23] Kluitenberg GJ, Heitman JL. Effect of forced convection on soil water content measurement with then dual-probe heat-pulse method. In: Smiles D, Raats PAC, Warrick A, editors. Heat and mass transfer in natural environment, the Philip volume. AGU, geophysical monograph series, no. 129.
[24] Mishra S, Parker JC. Parameter estimation for coupled unsaturated flow and transport. Water Resour Res 1989;25:385–96.
[25] Mori Y, Hopmans JW, Mortensen AP, Kluitenberg GJ. Multi-functional heat pulse probe for the simultaneous measurement of soil water content, solute concentration, and heat transport parameters. Vadose Zone J 2003;2:561–71.
[26] Mori Y, Hopmans JW, Mortensen AP, Kluitenberg GJ. Estimation of vadose zone water flux from multi-functional heat pulse probe measurement. Soil Sci Soc Am J, in press.
[27] Mortensen AP, Jensen KH, Nilsson B, Juhler RK. Multiple tracing experiments in unsaturated fractured clayey till. Vadose Zone J 2004;3:634–44.
[28] Noborio K, McInnes KJ, Heilman JL. Measurements of soil water content, heat capacity, and thermal conductivity with a single TDR probe. Soil Sci 1996;161:22–8.
[29] Nützmann G, Maciejewski S, Joswig K. Estimation of water saturation dependence of dispersion in unsaturated porous media: experiments and modelling analysis. Adv Water Res 2002;25:565–76.
[30] Ochsner TE, Horton R, Ren T. Simultaneous water content, air-filled porosity, and bulk density measurements with thermo-time domain reflectometry. Soil Sci Am J 2001;65:1618–22.
[31] Pot V, Šimůnek J, Benoit P, Coquet Y, Yra A, Martínez-Cordón M-J. Impact of rainfall intensity on the transport of two herbicides in undisturbed grassed filter strip soil cores. J Contam Hydrol, submitted for publication.
[32] Ren T, Noborio K, Horton R. Measuring soil water content, electrical conductivity, and thermal properties with a thermo-time domain reflectometry probe. Soil Sci Soc Am J 1999;63:450–7.
[33] Ren T, Kluitenberg GJ, Horton R. Determining soil water flux and pore water velocity by a heat pulse technique. Soil Sci Am J 2000;64:552–60.
[34] Ren T, Ochsner TE, Horton R. Development of thermo-time domain reflectometry for vadose zone measurement. Vadose Zone J 2003;2:544–51.
[35] Rhoades JD, Raats PAC, Prather RJ. Effects of liquid-phase electrical conductivity, water content, and surface conductivity on bulk soil electrical conductivity. Soil Sci Soc Am J 1976;40:651–5.
[36] Šimůnek J, Šejna M, van Genuchten MT. The HYDRUS-2D software package for simulating two-dimensional movement of water, heat, and multiple solutes in variably-saturated media, version 2.0, Rep IGCWMC-TPS-53, 251 pp. Int Ground Water Model. Cent, Colo Sch of Mines, Golden; 1999.
[37] Šimůnek J, Jacques D, Hopmans JW, Inoue M, Flury M, van Genuchten MTh. Solute transport during variably-saturated flow—inverse methods. In: Dane JH, Topp GC, editors. Methods of soil analysis, Part 1. Physical methods. 3rd ed. Madison, WI: SSSA; 2002. p. 1435–49 [Chapter 6.6].

[38] Sophocleous M. Analysis of water and heat flow in unsaturated–saturated porous media. Water Resour Res 1979;15:1195–206.
[39] Sun N-Z, Yeh WW-G. Coupled inverse problems in groundwater modeling. 1. Sensitivity analysis and parameter identification. Water Resour Res 1990;26:2507–25.
[40] Tarara JM, Ham JM. Measuring soil water content in the laboratory and field with dual-probe heat-capacity sensors. Agron J 1997;89:535–42.
[41] Toride N, Inoue M, Leij FJ. Hydrodynamic dispersion in an unsaturated dune sand. Soil Sci Soc Am J 2003;67:703–12.
[42] Tuli A, Denton MA, Hopmans JW, Harter T, MacIntyre JL. Multi-step outflow experiment: from soil preparation to parameter estimation. Land, Air and Water Resources Report No. 100037, University of California, Davis, CA 95616, USA, 2001.
[43] van Genuchten MTh. A closed-form equation for predicting the hydraulic conductivity of unsaturated soils. Soil Sci Soc Am J 1980;44:892–8.
[44] Vaz CMP, Hopmans JW, Macedo A, Bassoi LH, Wildenschild D. Soil water retention measurements using a combined tensiometer-coiled time domain reflectometry probe. Soil Sci Am J 2002;66:1752–9.
[45] Wang Q, Ochsner TE, Horton R. Mathematical analysis of heat pulse signals for soil water flux determination. Water Resour Res 2002;38(6). doi:10.1029/2001WR001089.
[46] Wraith JM, Or D. Nonlinear parameter estimation using spreadsheet software. J Nat Resour Life Sci Edu 1998;27:13–9.